Article:
Kanja, J., Mills, R., Li, X. et al. (2021) Non-contact measurement of the thickness of a surface film using a superimposed ultrasonic standing wave. Ultrasonics, 110. 106291. ISSN: 0041-624X

https://doi.org/10.1016/j.ultras.2020.106291

Ultrasonics 110 (2021) 106291

Contents lists available at ScienceDirect

Ultrasonics

journal homepage: www.elsevier.com/locate/ultras

Non-contact measurement of the thickness of a surface film using a superimposed ultrasonic standing wave

J. Kanja *, R. Mills, X. Li, H. Brunskill, A.K. Hunter, R.S. Dwyer-Joyce

The Leonardo Centre for Tribology, University of Sheffield, Sir Frederick Mappin Building, Mappin Street, Sheffield S1 3JD, UK

ARTICLE INFO

Keywords:
Surface layer thickness
Coating thickness
Superimposed standing wave
Continuous pulsing
Quarter wavelength

ABSTRACT

Most methods used to measure the thickness of thin liquid or solid surface films and coatings need access to the coated surface. In this work reflected ultrasonic pulses were used to measure a coating thickness from a solid back face. Piezoelectric transducers on the solid back face emitted ultrasound waves and received the waves that bounced off the front face. The magnitude of the reflected wave was dependent on the film thickness at the front face. Most pulse-echo ultrasonic approaches use the time-of-flight through the surface layer to determine its thickness. However, as the film becomes thinner, the reflected echoes overlap and there is often an acoustic mismatch between the solid and the surface film that reduces the signal strength. In this work, we propose the use of an ultrasonic continuously repeated chirp longitudinal wave to amplify the effect of the surface film. Multiple reflections interfere within the solid to form a superimposed standing wave whose amplitude spectrum is highly dependent on the surface film thickness thus overcoming the acoustic mismatch problem. Two bare 10 MHz piezoelectric elements were bonded to a 10 mm thick aluminium solid in a pitch-catch arrangement such that one continuously sends repeating chirp ultrasound waves and the other acts as the receiver. The transmitter was set to send a repeating chirp wave of 4 ms duration corresponding to the bandwidth of the transducer in order to maximise signal amplitude. The incident and reflected waves constructively and destructively interfere to form a superimposed standing wave within the solid. The solid/surface film to solid/air boundary condition frequency spectra ratio showed the film resonant frequency modes as minima. Using this technique epoxy coatings ranging from 70 μm to 350 μm were measured and showed a good correlation with independent measurements using a surface profilometer.

1. Introduction

There are many examples of functional thin surface film applied to engineering components such as; protective coating layers on automobiles, marine and submarine vessels, solid lubricant coatings on bearings, the oil distribution around a gearbox casing, the oil film that forms ahead of an approaching piston liner, diffusion coatings on jet engines, thermoset epoxy resins and fibre-reinforced plastics that coat storage tanks and pipes in chemical plants. On-demand inspection of these surface films allows for condition monitoring, the evaluation of risk of failure and maintenance procedures. Commercial quantitative non-destructive evaluation tools originating from physical principles such as magnetism, optical interferometry, surface profilometry, and photo thermal radiation have been successfully used to measure wet and dry surface film thicknesses [1]. Albeit having high precision, they all require direct access to the free surface layer in order to perform these measurements.

An ultrasonic spectroscopy technique can be used to overcome this need for access to the surface film (i.e. measuring from the back face of the coated solid). The reflection of an ultrasonic wave from an interface of interest and the embedded information that can be obtained from reflected ultrasonic waves has been useful in performing measurements on surfaces in difficult locations [2–7]. When a normal incident wave strikes a surface, some of the energy will be transmitted into the neighbouring component while the remaining energy will be reflected towards the wave source. Conventional ultrasound spectroscopy tools operate on this principle whereby a single burst of energy is sent to an interface of interest. The proportion of energy reflected is used in suitable mathematical models to characterise the conditions at the surface layer [8]. Where the surface layer is relatively thick in comparison to the solid to which it is adhered to, usually, the surface layer thickness is inferred from the time delay between the echoes reflected off the interface of interest and the surface layer. However, as the layer

* Corresponding author.
E-mail address: jkanja1@sheffield.ac.uk (J. Kanja).

https://doi.org/10.1016/j.ultras.2020.106291
Received 27 May 2020; Received in revised form 5 August 2020; Accepted 21 October 2020
Available online 26 October 2020

Nomenclature

α	Attenuation coefficient (Np/m)
ρ	Density (kg/m^3)
$\emptyset$	Phase change at the front face boundary
$\emptyset$'	Phase change at the transducer boundary
ω	Angular frequency ($\omega = 2\pi f$)
A	Amplitude of recorded wave signal (V)
A_0	Amplitude of driving wave signal emitted by transducer (V)
c	Wave speed (ms^{-1})
f	Frequency of ultrasonic wave (Hz)
k	Wave number (Hz·s/m)
L	Solid length (m)
P	Complex pressure amplitude (Pa)
p	Wave pressure (Pa)
R	Reflection coefficient at interface
R'	Reflection coefficient at the transducer boundary
S	Standing wave reflection coefficient
t	Time (s)
z	Specific acoustic impedance ($z = \rho c$)

becomes thinner the reflected echoes tend to overlap and a resonance method is employed to perform surface layer thickness calculations. This technique has proved to be successful in the thickness measurement of surface coatings [9–15], condensate film thickness [16–21] and oil film thickness especially in lubricated machine components [2–7].

Nonetheless, pulse-echo techniques have drawbacks of having the signal to noise ratio being reduced by phase measurement inaccuracies especially in highly attenuating solids and acoustic mismatch limiting transmission into the coating material. Continuous ultrasound waves on the other hand generate resonance frequencies and do not suffer from some of the limitations of pulse-echo approach. In this work we apply a continuous ultrasound wave measurement approach to detect and measure surface film thicknesses on a solid metal. The principle behind this method is to continuously send a repeating chirp ultrasound wave from a transducer located on the back face of a solid. Because the driving frequency is swept, various wavelengths are formed within the solid that give rise to various harmonics. The multiple waves inside the solid constructively and destructively interfere to form a superimposed standing wave. Each reflected echo serves to reinforce the superimposed standing wave. A resultant spectrum contains harmonics or resonance frequencies observed as a series of antinodes separated by the solid fundamental frequency and their location is strongly governed by the solid and surface layer geometric and material properties. The use of multiple echoes to increase ultrasonic film thickness measurement sensitivity has been theoretically and experimentally demonstrated where an increase in the number of reflected echoes gave a more accurate measurement of the film resonant frequency [22]. The standing wave amplitude and phase is therefore highly sensitive to the conditions at the interface. This eliminates the need to wait for the reflected echoes to characterise surface layers due to the almost instantaneous response of the system. Recently, a continuously repeating ultrasound chirp technique has been successfully used to measure the viscosity of lubricating oils at a solid-oil interface using an acoustic matching layer [23].

2. Background

When a bulk ultrasound wave of a known frequency, f strikes a boundary between two materials at normal incidence, reflection occurs. The reflection coefficient magnitude, R will depend on the nature of the interface. When two materials are perfectly bonded together, at normal incident angle, the wave is partly transmitted into the second medium and partly reflected. With an assumption of a perfect interface at boundary $x = 0$ for a two layered media as illustrated in Fig. 1a, it follows from continuity of pressure and velocity that the reflection coefficient in terms of impedance Z is:

$$R_{1,2} = R = \frac{z_2 - z_1}{z_2 + z_1} \tag{1}$$

where $R_{1,2}$ denotes wave travelling from material 1 to 2. The subscripts i, r and t stand for incident, reflected and transmitted waves respectively and a and b stand for transmitted and reflected waves respectively in medium 2.

If a sound wave is reflected at a boundary between an acoustically dense medium to an acoustically denser medium, i.e. the limit $z_1/z_2 \to 0$, the reflected wave has the same amplitude as the incident wave with no phase change. If it is reflected vice versa, i.e. $z_1/z_2 \to \infty$, then $\emptyset = \pi$.

A negative R sign shows a reversal of the phase in relation to the incident wave. A positive value of R shows that the incident and reflected waves are in phase. For a free boundary, i.e. aluminium and air boundary, where $z_1/z_2 \to \infty$ practically all the wave is reflected. The value of R tends towards 1, the amplitude of the incident wave is equal to that of the reflected wave.

When an incident wave arrives at a boundary between two layers as illustrated in Fig. 1b, some of the wave is reflected into layer 1 and some of the wave is transmitted into layer 2. The transmitted wave propagates through layer 2 of uniform thickness and reaches the boundary $x = h$. At this boundary, some of the wave will be reflected into layer 2 and some will be transmitted into layer 3. The echoes from the boundary between medium 1 and medium 2, and the boundary between medium 2 and medium 3 travel back to the boundary$x = 0$ and the process is repeated. Where the time period of the incident signal is less than $2h/c_2$, the echoes in medium 1 and 3 are separated by time $2h/c_2$. Where the incident signal has a duration greater than $2h/c_2$ then:

$$p_i = P_i e^{i(\omega t - k_1 x)} \tag{2}$$

$$p_r = P_r e^{i(\omega t + k_1 x)} \tag{3}$$

$$p_a = A e^{i(\omega t - k_2 x)} \tag{4}$$

$$p_b = B e^{i(\omega t + k_2 x)} \tag{5}$$

$$p_t = P_t e^{i(\omega t - k_3 x)} \tag{6}$$

where k_1, k_2 and k_3 represent the wave number in medium 1, 2 and 3, respectively. Continuity of impedance at $x = 0$ and $x = h$ together with algebraic manipulation gives a pressure reflection coefficient (for a full description refer to Kinsler et al. [24]):

$$R_{layer} = \frac{\left(1 - \frac{z_1}{z_3}\right) cosk_2 h + i\left(\frac{z_2}{z_3} - \frac{z_1}{z_2}\right) sink_2 h}{\left(1 + \frac{z_1}{z_3}\right) cosk_2 h + i\left(\frac{z_2}{z_3} + \frac{z_1}{z_2}\right) sink_2 h} \tag{7}$$

where h is the thickness of layer 2 and $k_2 = \omega/c_2$. Chen et al. [18] show the relationship between f and surface layer thickness such that spectral peaks are observed when $k_2 h = (n + 1/2)\pi$ where n is any integer. Therefore when $k_2 h = \pi/2$ for resonant frequency i.e. ($f = f_0$):

$$\frac{\pi}{2} = \frac{2\pi f_0 h}{c_2} \tag{8}$$

Rearranging Eq. (8) gives:

$$h = \frac{c_2}{4 f_0} \tag{9}$$

For other resonant modes (i.e. $n \geq 1$) Eq. (9) can be rewritten as:

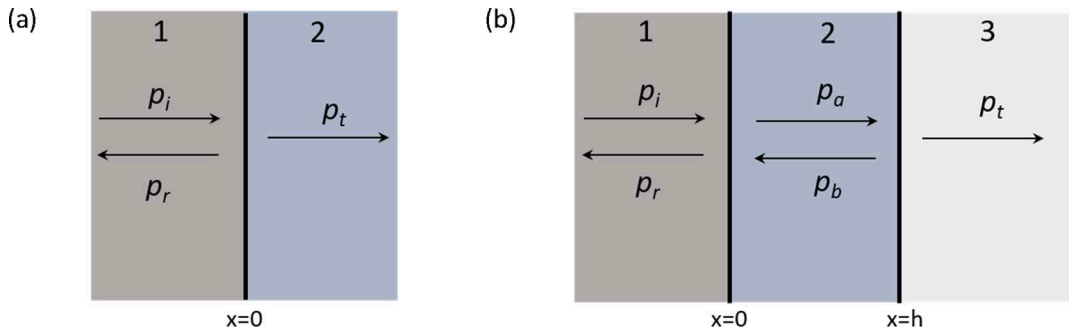

Fig. 1. (a) Reflection and transmission of a wave normally incident at a boundary between two materials for two layered media and (b) three layered media.

$$h = \frac{c_2(2n+1)}{4f_n} \tag{10}$$

3. Superimposed standing wave

In this work we apply the laws of reflection for a single frequency to the multiple waves responsible for the creation of a standing wave. When multiple waves superimpose, a standing wave is created that is the summation of the respective wave interactions for each reflection. The following equations are therefore true for the constituent waves that give rise to the standing wave and how they are influenced by the presence of a surface layer on an interface of interest.

When propagating through a material, an ultrasonic wave of a known frequency will be attenuated as a function of material attenuation coefficient, α, and length, L, using $A = A_0 e^{L\alpha}$. When the ultrasonic wave reaches a boundary, it will be reflected along the incident wave path returning it to the source of the original wave upon which it will further be reflected. Fig. 2 shows a schematic of an ultrasound wave path as it is reflected within the material multiple times.

Immediately before the first reflection at the interface of interest occurs, the incident wave has been attenuated and the waveform amplitude is given by:

$$A_0 e^{i\omega(\frac{L}{c}-t)} e^{L\alpha} \tag{11}$$

Immediately after the first reflection, the amplitude is given by:

$$A_0 e^{i\omega(\frac{L}{c}-t)} e^{L\alpha} R e^{-i\varnothing} \tag{12}$$

where $Re^{-i\varnothing}$ is the complex form of the reflection coefficient (Eq. (1)) at the interface of interest. The wave then passes back through the solid and towards the source (transducer) and immediately before the reflection at the transducer interface, the amplitude is given as:

$$A_0 e^{i\omega(\frac{2L}{c}-t)} e^{2L\alpha} R e^{-i\varnothing} \tag{13}$$

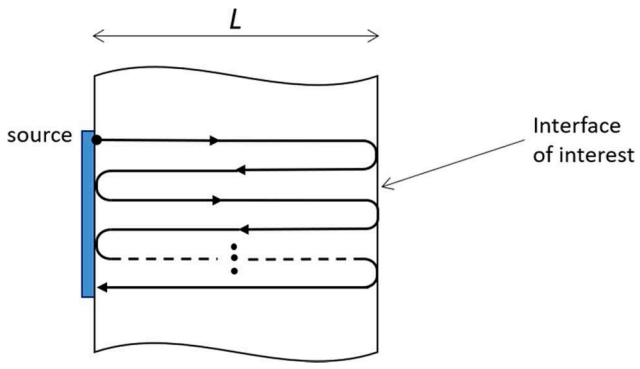

Fig. 2. Schematic showing incident wave and subsequent reflection paths within a solid.

The amplitude immediately after the reflection at the boundary at the transducer interface is given by:

$$A_0 e^{i\omega(\frac{2L}{c}-t)} e^{2L\alpha} R e^{-i\varnothing} R' e^{-i\varnothing'} \tag{14}$$

where $R'e^{-i\varnothing'}$ is the complex form of the reflection coefficient at the transducer interface boundary. Successive reflection continues until the wave decays to zero, which is governed by the attenuation coefficient. If we describe a passage as consisting of travel from the transducer to the interface and back again, we can represent the amplitude of the wave after n passages as:

$$A_0 e^{i[\omega(\frac{2nL}{c}-t)-n\varnothing-(n-1)\varnothing']} e^{2nL\alpha} R^n R'^{(n-1)} \tag{15}$$

At the transducer, all the successive reflected waves will superimpose to set up a standing wave in the solid, and the standing wave amplitude, at a given frequency, is given as:

$$A = A_0 \sum_{n=1}^{\infty} e^{i[\omega(\frac{2nL}{c}-t)-n\varnothing-(n-1)\varnothing']} R^n R'^{(n-1)} e^{2nL\alpha} \tag{16}$$

This is illustrated in Fig. 3. Constructive and destructive interferences cause nodes and antinodes in the standing wave. The standing wave formed has spatially varying amplitudes as a result of wave attenuation through the solid.

For a solid-air boundary, $R = 1$ and $\varnothing$=0, thus the amplitude is given by:

$$A_{solid-air} = A_0 \sum_{n=1}^{\infty} e^{i[\omega(\frac{2nL}{c}-t)-(n-1)\varnothing']} R'^{(n-1)} e^{2nL\alpha} \tag{17}$$

When there is an air-backed surface layer present at the boundary, R is obtained from Eq. (7) therefore:

$$A_{solid-surfacelayer} = A_0 \sum_{n=1}^{\infty} e^{i[\omega(\frac{2nL}{c}-t)-n\varnothing-(n-1)\varnothing']} R^n R'^{(n-1)} e^{2nL\alpha} \tag{18}$$

The ratio of the standing wave amplitudes, S, can be defined as:

$$S = \frac{A_{solid-surfacelayer}}{A_{solid-air}} = \frac{\sum_{n=1}^{\infty} e^{i[\omega\left(\frac{2nL}{c}-t\right)-n\varnothing-(n-1)\varnothing']} R^n R'^{(n-1)} e^{2nL\alpha}}{\sum_{n=1}^{\infty} e^{i[\omega(\frac{2nL}{c}-t)-(n-1)\varnothing']} R'^{(n-1)} e^{2nL\alpha}} \tag{19}$$

Because S is periodic with time, taking a signal root mean square (RMS) provides a DC response of the system. S, when plotted against frequency, reveals surface layer harmonics at regular frequency intervals governed by Eq. (8). As a result, this allows for the simulation of a solid-surface layer interface situation of known surface layer thickness.

Since the frequency that will cause resonance within a surface layer is not known in advance, the equivalent driving frequency is not known. Because of this, sweeping through a series of frequencies, also known as a chirp (Fig. 6a), and recording the responses for all is more convenient. The attenuation coefficient is dependent on frequency therefore the various frequencies in the sweep will be attenuated differently as they propagate through the solid [25]. However, because the superimposed

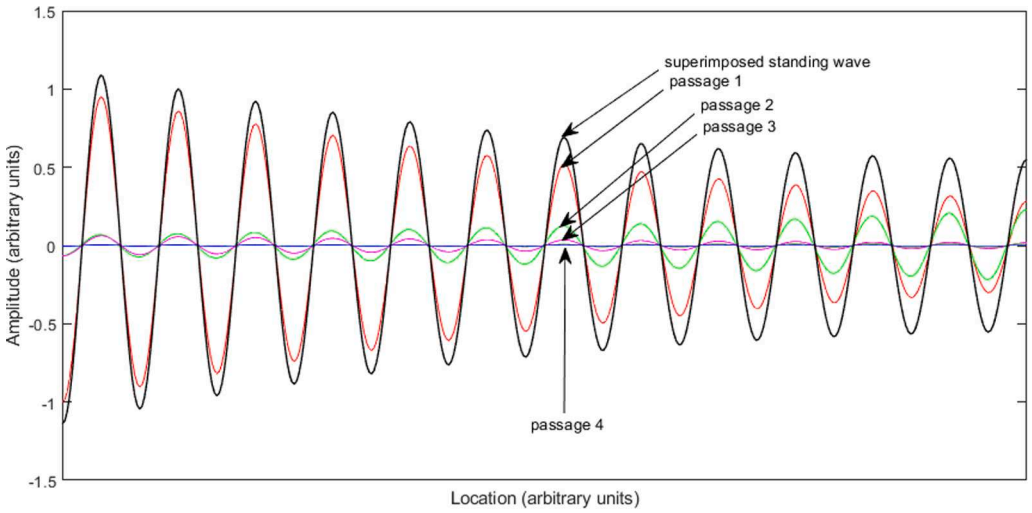

Fig. 3. Schematic illustrating superposition of a series of single frequency ultrasonic wave reflections within a solid.

standing wave that is formed is a summation of the individual waveforms within the solid, the compound effect of attenuation coefficient only serves to either reduce or increase the standing wave amplitudes depending on the solid acoustic properties. From Eq. (19), it can be noted that the effect of attenuation coefficient normalises out and the measurement of surface film thickness remains unaffected by the dependence of attenuation coefficient on frequency.

A superimposed standing wave frequency response for a 20 MHz frequency chirp wave was modelled in MATLAB® software from Eqs. (7) and (19) for a 138 μm thick solid epoxy film on a 10 mm thick semi-infinite aluminium plate using the model inputs outlined in Table 1.

The respective reflection coefficients R and R' at each angular frequency were calculated and the wave summation was performed for thirty reflections. After thirty reflections the frequency response was at its maximum and there were no significant changes with increased number of reflections. The signal was considered to have attenuated to background levels. The frequency responses for solid/air and solid/epoxy boundary conditions and the associated S plot were plotted in Fig. 5 and an interference pattern was observed. A surface layer causes a reduction in R and a change in $\emptyset$ relative to the solid/air boundary condition. This changes the coherent standing wave resonant frequencies such that, when the solid/layer and solid/air boundary conditions are compared, a reduction in amplitude and change in frequency is observed and furthermore, the surface layer resonance is now

Table 1
Model input parameters.

	Material properties			**Units**
z_1	Aluminium acoustic impedance		16.8×10^6	Rayl
z_2	Acoustic impedance	Epoxy for R condition	3.15×10^6	Rayl
		Transducer for R' condition	33.7×10^6	Rayl
z_3	Air acoustic impedance		384	Rayl
c_2	Surface film longitudinal acoustic velocity	Epoxy for R condition	2670	m/s
		Transducer for R' condition	4350	m/s
h	Surface film thickness	Epoxy for R condition	138×10^{-6}	m
		Transducer for R' condition	2×10^{-4}	m
L	Aluminium thickness		0.01	m
c	Aluminium longitudinal acoustic velocity		6211	m/s
Ultrasound chirp wave input				
f	Frequency		0: 1 MHz: 20 MHz	
n	Number of reflections		1:30	

superimposed on the standing wave. The first order peaks were separated by Δf_s, where Δf_s was the separation between the first order peaks of the solid/air and solid/epoxy frequency spectra. The second order by $2\Delta f_s$ and the mth order by $m\Delta f_s$. Eventually, when the m^{th} separation was equal to f_s the peaks were back in phase. A zoomed in figure from 0 MHz to 15 MHz along the x-axis was plotted to better illustrate this interference as shown in Fig. 4 (top). This pattern was observed to be periodic around $m\Delta f_s = f_s$.

It was also observed that some solid resonance peaks were missing as a result of the epoxy layer. These resonances, in practise, act as the driving frequencies that force the epoxy layer to resonate. From the modelling, it was observed that these occur at $f_0 = 4.8$ MHz and $3f_0 = 14.41$ MHz. The extraction of the first harmonic has been shown by the blue rectangle in Fig. 4. The best signal to noise ratio was obtained around these frequencies where there was a maximum change in amplitude and a plot of S showed corresponding minimum point (Fig. 4 (bottom)). A MATLAB® envelope function was applied, for convenience, to confirm these frequencies as the lowest resonance dip points (minima) as shown in Fig. 5b.

However, from Eqs. (9) and (10), calculations showed that the epoxy layer naturally resonates at $f_0 = 4.84$Mhz and $3f_0 = 14.51$ Mhz where a frequency span of 0 Mhz to 20 MHz was used. From this observation, it is thought that the driving frequency that causes the epoxy layer to resonate is dependent on the frequency components of the superimposed standing wave.

The epoxy layer thickness can be calculated at any of the harmonics but a more convenient method, especially where multiple resonant dips occur within the frequency bandwidth, is to take half the interval spacing between adjacent dips and averaging these to give $f_{average}$. This been reported in literature [18,26]. Eq. (10) can therefore be simplified as:

$$h = \frac{c_2}{4f_{average}} \tag{20}$$

4. Experimental methodology

In this work, a driving frequency sweep (Fig. 6a) was continuously repeated and superimposed with its reflections to create a superimposed standing wave. Each successive reflection served to reinforce the standing wave. At certain points in time that directly relate to specific driving frequencies, antinodes occurred due to constructive interference and the pressures are maximum at these locations, whereas nodes occurred due to destructive interferences and pressures at these locations are zero. Because piezoelectric transducers have a finite

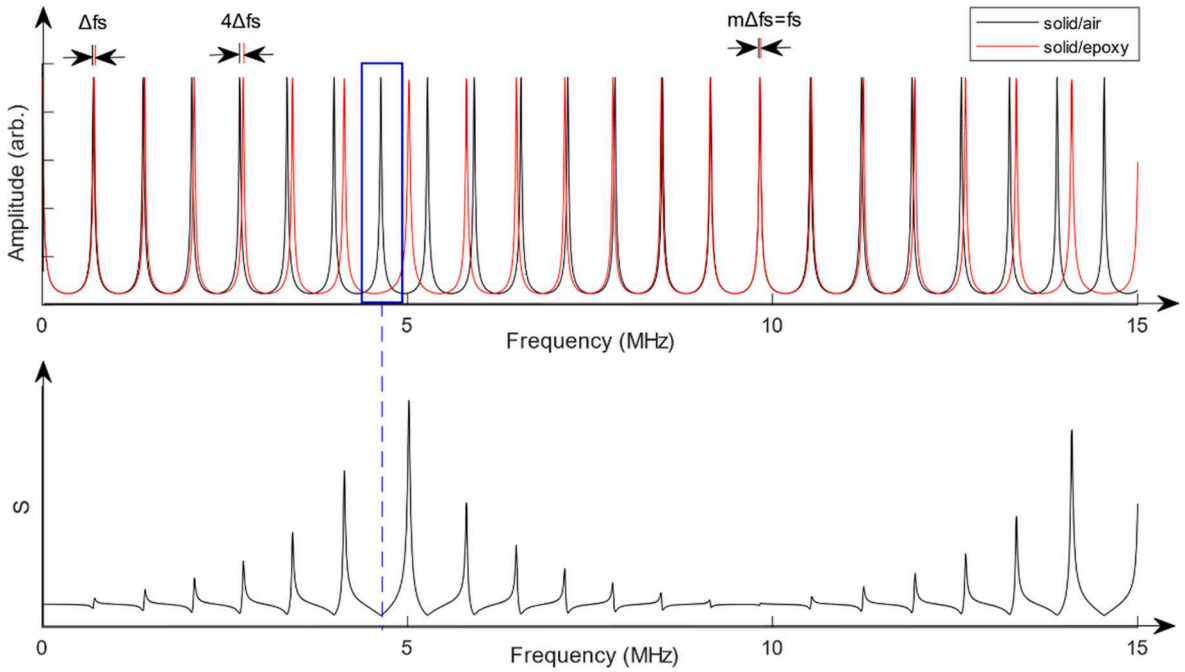

Fig. 4. (Top) Zoomed in superimposed standing wave frequency responses showing the peak separation pattern and (bottom) the extraction of epoxy resonant frequency from the S plot.

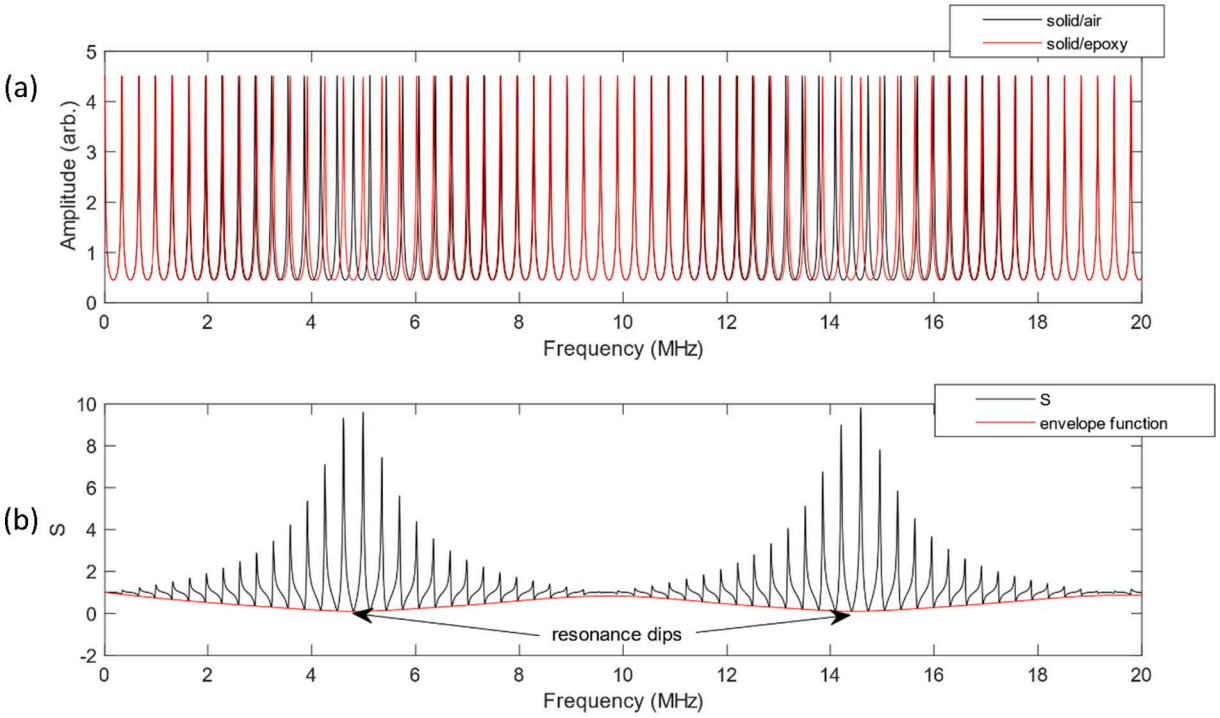

Fig. 5. Mathematical model spectra showing (a) the superimposed standing wave frequency response and (b) the S of a 138 μm epoxy layer.

bandwidth, they cannot generate or receive a full range of frequencies (Fig. 6b). A typical response from a transducer is as shown in Fig. 6c where the lower and higher frequencies are attenuated. The antinodes when analysed in the frequency domain are separated by the solid fundamental frequency, f_{solid}.

5. Experimental apparatus and signal processing

An experiment was performed at a constant room temperature where a Picoscope 5442b USB oscilloscope was used as an arbitrary function generator and signal digitiser and to relay the data to a laptop PC. The laptop PC was used for data storage and processing. The oscilloscope was controlled via the PC using a bespoke LabVIEW software. This arrangement provides simple and cheap instrumentation; because the pulsing and receiving circuits are separate there is no need for specialist ultrasonic pulsing apparatus.

An aluminium plate of 10 mm thickness was used as the test solid. Two bare 10 MHz resonant frequency wrap-around longitudinal

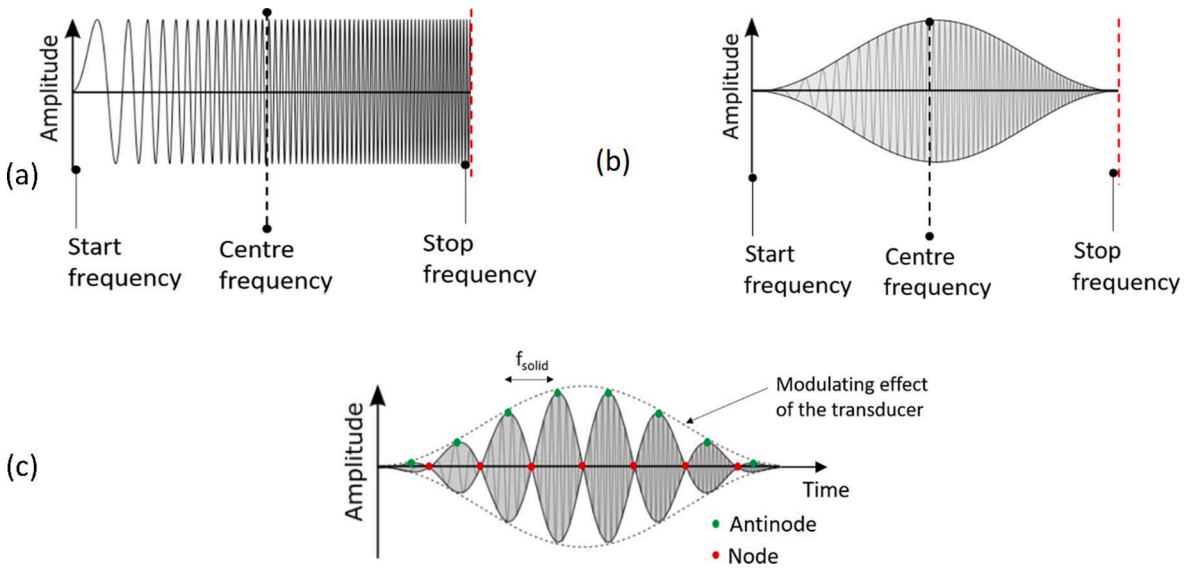

Fig. 6. (a) A schematic illustration of one positively chirped frequency sweep. (b) Schematic illustration showing modulating effect of the transducer. (c) Schematic illustration showing the combined transducer and interference modulating effect.

piezoelectric transducers were coupled to the solid using a permanent adhesive couplant in a pitch-catch arrangement. The pitch-catch configuration allowed for the continuous pulse transmitting (Tx) and receiving (Rx) of ultrasound waves signals simultaneously. A schematic of the setup is as shown in Fig. 7.

The transmitter was continuously excited by a sinusoidal varying voltage. This resulting longitudinal mechanical wave propagated through the solid, was reflected from the interface of interest, and the wave that arrived at the receiver was converted to an analogue voltage signal. The incident and reflected waves superimposed within the solid to form a standing wave. Upon demand, the standing wave ultrasound signals were then acquired by the receiver and relayed to the oscilloscope for digitizing. The superimposed standing wave frequency components were governed by the material properties, the source frequency, and the surface layer properties.

A 4 V peak-to-peak positively chirped ultrasound wave of 10 MHz centre frequency and 19 MHz sweep span for a duration of 4 ms was sent from the transducer and into the solid, and then continuously repeated. The sample rate was 8 ns. The characteristics of the chirp wave were such that its centre frequency was operated at the transducer resonant frequency, the frequency span lay within the transducer working bandwidth limits and that the sweep time was enough to allow sweeping across the various frequencies in the chirp wave. When sweeping through the frequencies, the individual frequency residence time was small enough to allow the standing wave resonances to be equally spaced.

6. Results

Fig. 8a shows a measured ultrasound signal that was acquired for a superimposed standing wave for the solid-air condition. It showed an interference pattern due to multiple reflection within the solid and transducer modulating effects as previously explained (refer to Fig. 6c). Fig. 8b shows a Fast Fourier Transform (FFT) of the measured signal that revealed the amplitude and frequency components of the superimposed standing wave. The solid fundamental frequency f_{solid} was 306 kHz. A secondary spectrum peak was also observed in the range 10–14 MHz. With a transducer thickness of 0.2 mm and an acoustic velocity of 4350 ms^{-1} the transducer fundamental frequency was calculated as 10.9 MHz and this was thought to cause the secondary peak.

A planar epoxy layer was applied to the surface and left to cure overnight. The epoxy thickness was measured using a 3D surface profilometer by running the profilometer from the coated to an uncoated region and found to be 138 μm.

A superimposed standing wave measurement for solid/epoxy layer boundary condition was acquired and an FFT was applied to give the frequency response. The solid/air and solid/epoxy frequency spectra were compared as shown in Fig. 9. Presence of an epoxy layer at the interface of interest caused some of the wave energy to be transmitted into the layer (Fig. 1b) and as such the amplitude of the solid standing wave (Fig. 9) reduced and some frequencies were lost or shifted along the horizontal axis. *S* when plotted against frequency (Fig. 9b) revealed regions of epoxy resonances observed as dips.

The mathematical modelling of a 138 μm epoxy layer as shown in Fig. 5 showed a similar pattern in the frequency spectra and *S* plots when compared to the experimental data as shown in Fig. 9. The location of

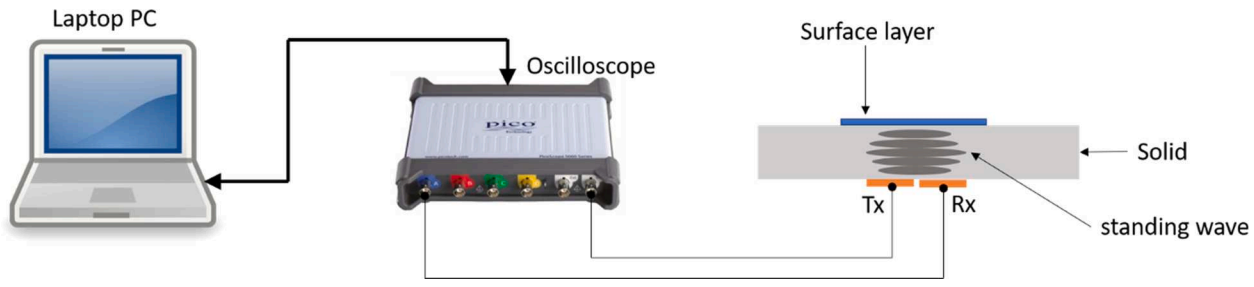

Fig. 7. Schematic of experimental arrangement.

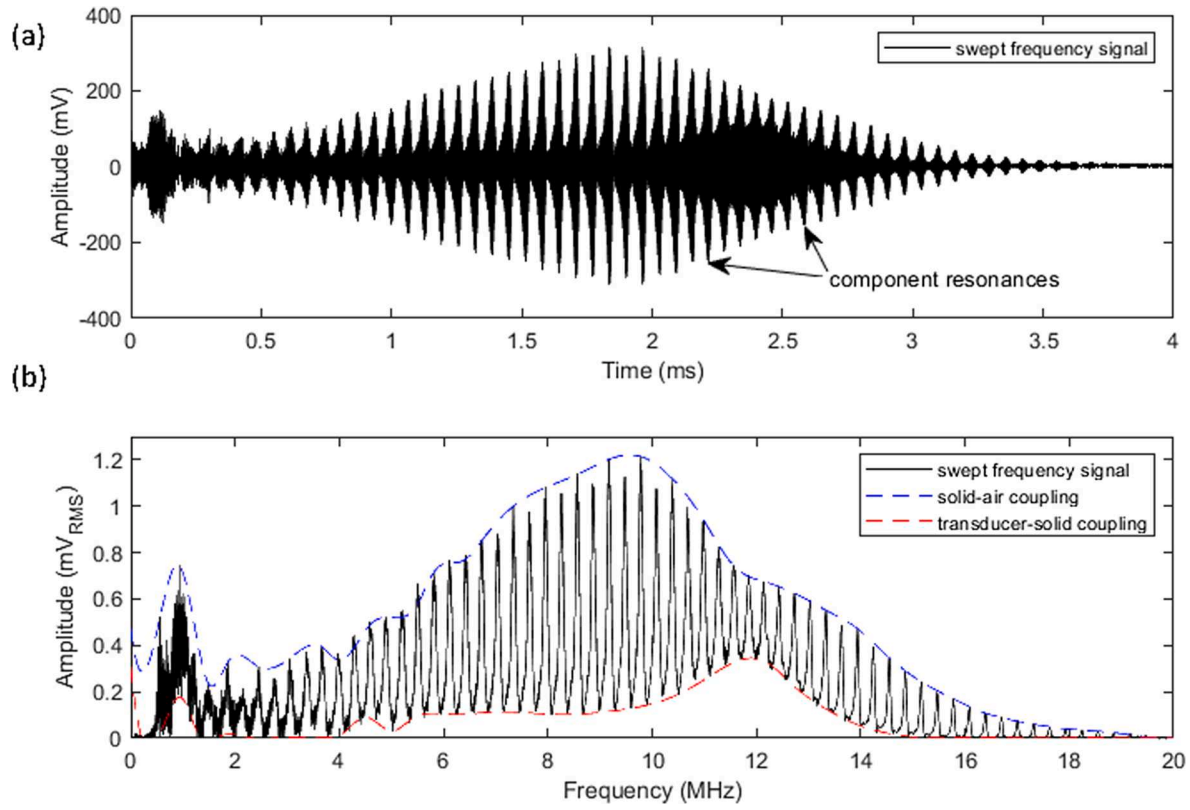

Fig. 8. (a) A time domain spectrum of the acquired measurement signal showing the superimposed standing wave with modulating effects as illustrated in Fig. 6. The peaks represent the solid resonances. (b) A frequency domain composite spectrum of the measured signal.

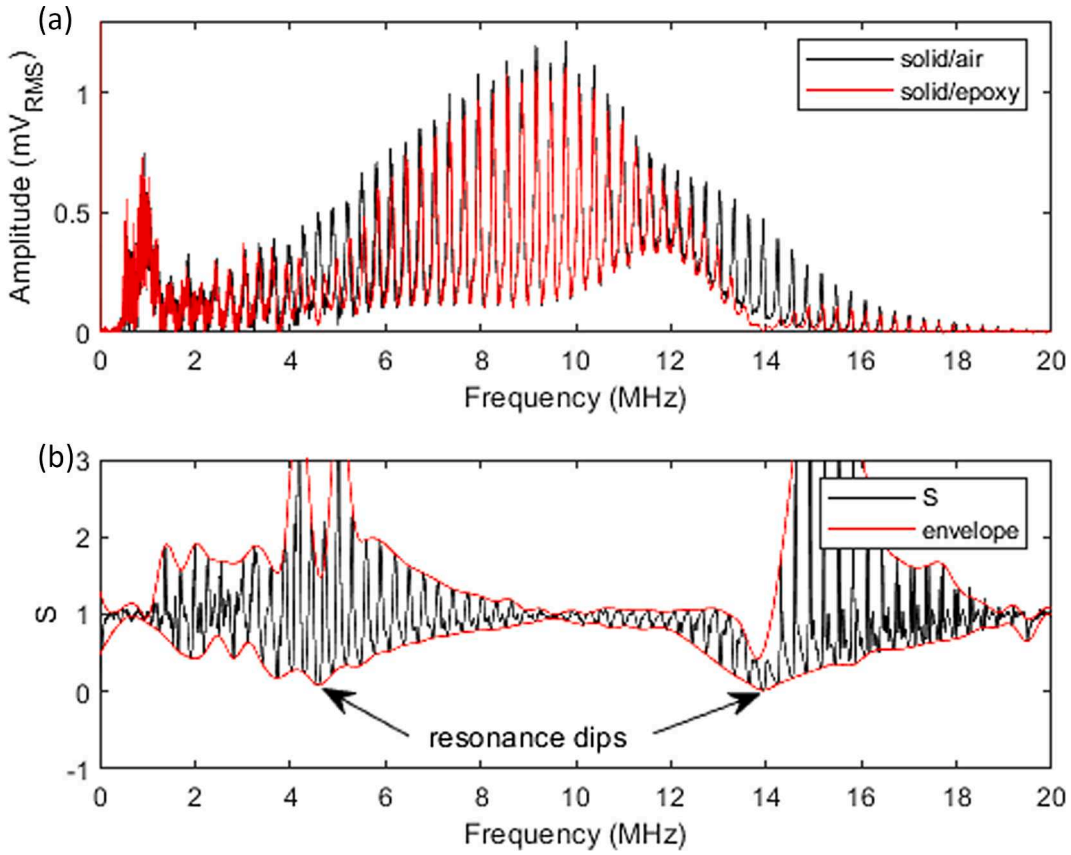

Fig. 9. (a) A Frequency domain plot showing solid/air and solid/epoxy boundary conditions. (b) With their associated standing wave reflection coefficient.

the resonance dips was identical. The experimental epoxy resonance frequency modes were observed at 4.58 MHz and 13.9 MHz, respectively. The frequency difference was averaged, and the experimental thickness was calculated as 143 μm. This showed a 3.6% difference from the profilometer measurement.

A further four different epoxy layer thicknesses were manufactured and measured. The centre frequency of the chirp was set to 10 MHz and the sweep span was adjusted to 14 MHz to eliminate the noise observed at frequencies below 3 MHz as seen in Fig. 9. The respective frequency domain and *S* spectra were used to identify the epoxy layer resonant frequency modes as shown in Fig. 10. Where a single resonance dip was observed within the transducer bandwidth (Fig. 10a) the resonant frequency was taken at that location. For multiple dips (Fig. 10 b, c and d) the frequency difference between adjacent dips was averaged.

A comparison was done between the ultrasonic and profilometer techniques as shown in Fig. 11. There was a good correlation between ultrasound and contact profilometer measurements. The profilometer measurement errors increased with increasing thickness with the lowest and highest errors being 2.65% and 6.90% respectively. It was observed that the ultrasound measurements gave higher thickness calculations than the measured profilometer readings. The highest percentage error was 12.6% and the lowest was 6.87%.

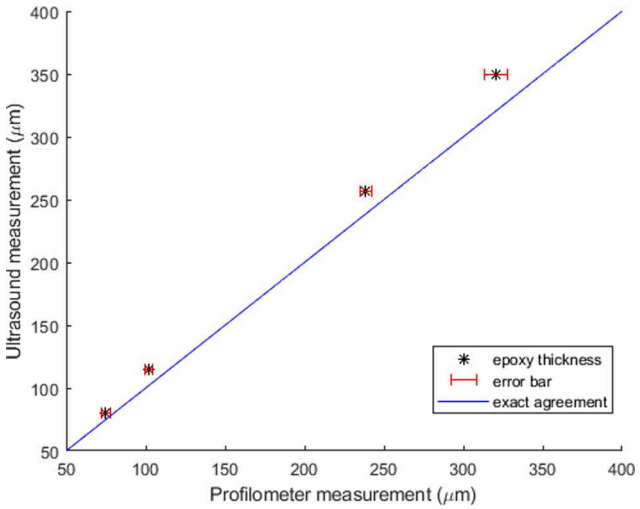

Fig. 11. Comparison between ultrasound and profilometer measurements.

7. Discussion

The experiments were performed at room temperature so any temperature effects on the solid and epoxy geometric and structural properties were negligible. A significant temperature change in both the metal solid and the surface film would result in linear thermal expansion which would in turn affect the solid resonance peak locations. To perform thickness measurements at elevated temperatures, the metal solid must be calibrated. However, the piezoelectric transducer material could be operated at elevated temperatures and therefore remained unaffected by any temperature change.

It was also assumed that the thickness of the adhesive couplant was negligible and that the boundary between the solid and the epoxy layer was perfect. In reality this is not the case. The presence of an intermediate layer between the transducer and the solid would introduce some acoustic damping depending on the adhesive thickness. In this work the adhesive used was of low viscosity and during the bonding process enough pressure was applied on the transducers to ensure a very thin film in the order of < 5 μm but not so much as to damage them. This resulted in asperity contact between the transducer and the metal to

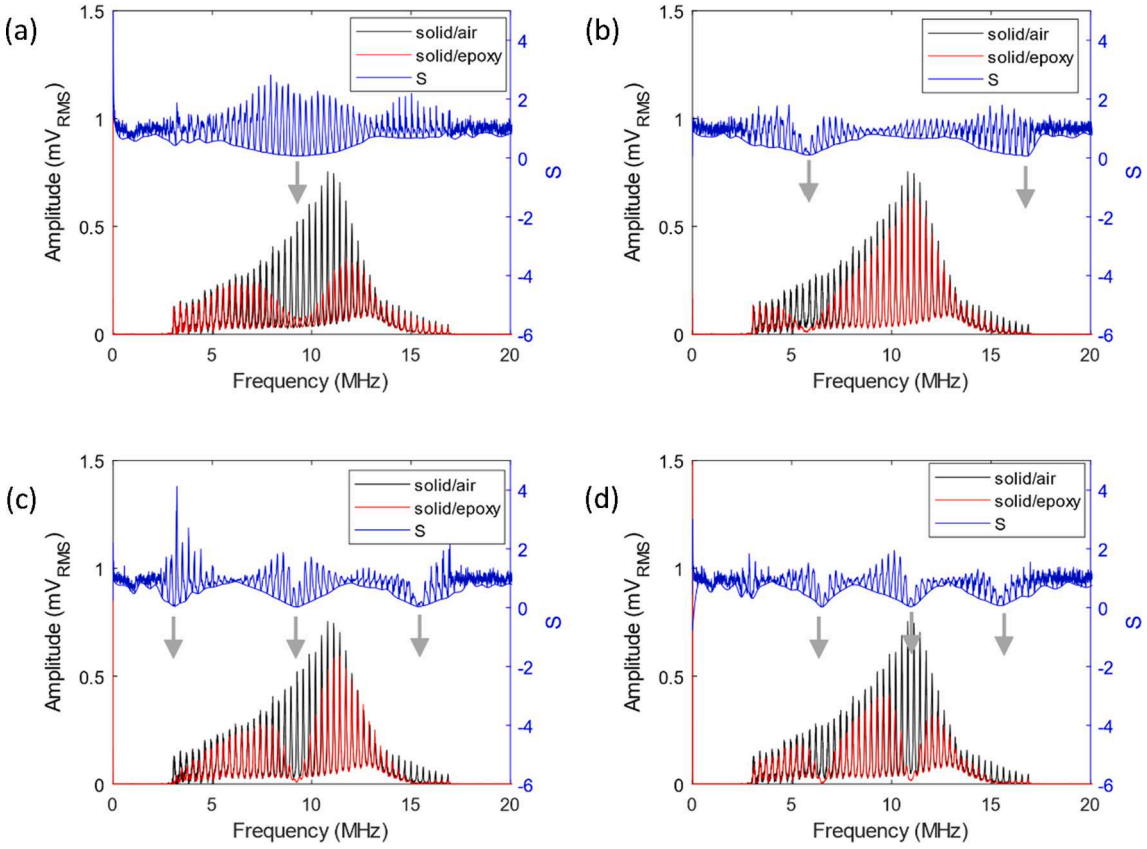

Fig. 10. Frequency domain spectra showing solid/air and solid/epoxy boundary conditions with their corresponding S plots for four epoxy thicknesses in order of increasing thickness from (a) to (d). The arrows identify the resonance dips with their associated resonant frequency mode locations.

allow a smooth transition of ultrasonic energy.

There were no air gaps in the epoxy layer after the curing process and it was assumed that the asperity contact between the epoxy and the metal was perfect to allow for a clean ultrasound transmission. Inhomogeneities within the metal were assumed to be negligible. Irregularities in the structures would affect sound transmission and propagation and ultimately lead to measurement inaccuracies

The epoxy layers were not entirely planar and because of this the profilometer thickness extraction were performed at a position perpendicular to the sensors. This region had the greatest ultrasound sensitivity. The epoxy thickness results therefore represent localised thicknesses. For a complete epoxy layer profile thickness measurement, sensor arrays could be used separated at known intervals. This would allow for a detailed ultrasonic mapping of the epoxy thickness for a defined section. Discrepancies arose due to the epoxy acoustic velocity being slightly different for each epoxy thickness.

It is worth noting that this superimposed standing wave measurement technique can only be applied where the film resonances lie within the operational transducer bandwidth. In this study, where the bandwidth was maximised by sending a 19 MHz chirp wave, the lower resonance boundary detectable would be 19.5 MHz which would give an epoxy thickness of 34 μm. The practicality of using higher frequency sensors to achieve a higher resonance boundary is limited by high sound attenuation in the materials with increasing frequency and decreased sensor robustness as it gets thinner. However, contemporary sputtering technology has been used to manufacture thin film elements that exhibit increased measurement resolution and signal strength.

8. Conclusions

This work presents the novel application of using a superimposed standing wave that is formed by continuously sending repeating positively chirped ultrasound waves for film thickness measurement of solid epoxy coatings on free surfaces. The multiple reflections within the solid reinforced the superimposed standing wave which made the response highly sensitive to changes occurring at the interface as compared to the traditional pulse-echo technique. Epoxy film thicknesses ranging from 70 μm to 350 μm were measured and showed a strong correlation with independent profilometer measurements.

This novel technique can be practically implemented in condition monitoring of surface films in difficult locations. Mathematical modelling can be compared with real-time ultrasound measurements to establish the film thickness thereby reducing downtime that would be required to open and access these layers. Additionally, the equipment used to perform these ultrasound measurements are low cost, have stand-alone capabilities and can be retrofitted to fit almost any real-life engineering component. They can also be easily modified to allow remote access on demand.

Declaration of Competing Interest

The authors declare that they have no known competing financial interests or personal relationships that could have appeared to influence the work reported in this paper.

Acknowledgements

The authors would like to acknowledge the financial support of the Engineering and Physical Sciences Research Council for funding this research through Dwyer-Joyce's fellowships on *Tribo-Acoustic Sensors* EP/N016483/1 and the *Centre for Doctoral Training in Integrated Tribology* EP/L01629X/1.

Appendix A. Supplementary data

Supplementary data related to this article can be found online at https://doi.org/10.17632/mcg9xtmzjw.3.

References

[1] B.S.I. BSI, "Paints and varnishes - Determination of film thickness (ISO 2808: 2019)," 2019.
[2] R.S. Dwyer-Joyce, D.A. Green, P. Harper, R. Lewis, S. Balakrishnan, P.D. King, H. Rahnejat, S. Howell-Smith, The measurement of liner - Piston skirt oil film thickness by an ultrasonic means, SAE Technical Papers (2006).
[3] T. Reddyhoff, R.S. Dwyer-Joyce, J. Zhang, B.W. Drinkwater, Auto-calibration of ultrasonic lubricant-film thickness measurements, Meas. Sci. Technol., 19(4), 2008.
[4] R.S. Dwyer-Joyce, T. Reddyhoff, B. Drinkwater, Operating limits for acoustic measurement of rolling bearing oil film thickness, Tribol. Trans. 47 (3) (2004) 366–375.
[5] R.S. Dwyer-Joyce, P. Harper, B.W. Drinkwater, A method for the measurement of hydrodynamic oil films using ultrasonic reflection, Tribol. Lett. 17 (2) (2004) 337–348.
[6] R. Mills, E. Avan, R.S. Dwyer-Joyce, Piezoelectric sensors to monitor lubricant film thickness at piston–cylinder contacts in a fired engine, Proc. Inst. Mech. Eng. Part J J. Eng. Tribol. 227 (2) (2012) 100–111.
[7] R.S. Dwyer-Joyce, B.W. Drinkwater, C.J. Donohoe, The measurement of lubricant-film thickness using ultrasound, Proc. R. Soc. Lond. 459 (2003) 957–976.
[8] R.S. Dwyer-Joyce, The application of ultrasonic NDT techniques in tribology, Proc. Inst. Mech. Eng. Part J J. Eng. Tribol. 219 (5) (2005) 347–366.
[9] A.I. Lavrentyev, S.I. Rokhlin, An ultrasonic method for determination of elastic moduli, density, attenuation and thickness of a polymer coating on a stiff plate, Ultrasonics 39 (3) (2001) 211–221.
[10] L. Ming-Xuan, W. Xiao-Min, M. Jie, Thickness Measurement of a Film on a Substrate by Low-Frequency Ultrasound, Chinese Phys. Lett. 21 (5) (2004) 870–873.
[11] R.S. Dwyer-Joyce, N. Hankinson, An ultrasonic technique for the measurement of elastic properties of soft surface coatings, Tribol. Int. 39 (4) (2006) 326–331.
[12] I. Alig, H. Oehler, D. Lellinger, S. Tadjbach, Monitoring of film formation, curing and ageing of coatings by an ultrasonic reflection method, Prog. Org. Coatings 58 (2–3) (2007) 200–208.
[13] S. Lemlikchi, J. Martinsson, A. Hamrit, H. Djelouah, M. Asmani, J. Carlson, Ultrasonic characterization of thermally sprayed coatings, J. Therm. Spray Technol. 28 (3) (2019) 391–404.
[14] H. Tohmyoh, M. Suzuki, Measurement of the coating thickness on the back side of double-sided coated structures by means of acoustic resonant spectroscopy, Surf. Coatings Technol. 204 (4) (2009) 546–550.
[15] S. Dixon, B. Lanyon, G. Rowlands, Coating thickness and elastic modulus measurement using ultrasonic bulk wave resonance, Appl. Phys. Lett., 88(14), 2006.
[16] Q. Lu, N.V. Suryanarayana, C. Christodoulu, Film thickness measurement with an ultrasonic transducer, Exp. Therm. Fluid Sci. 7 (4) (1993) 354–361.
[17] P.C. Pedersen, Z. Cakareski, J.C. Hermanson, Ultrasonic monitoring of film condensation for applications in reduced gravity, Ultrasonics 38 (1) (2000) 486–490.
[18] Z.Q. Chen, J.C. Hermanson, M.A. Shear, P.C. Pedersen, Ultrasonic monitoring of interfacial motion of condensing and non-condensing liquid films, Flow Meas. Instrum. 16 (6) (2005) 353–364.
[19] J.T. Kimball, M.R. Bailey, J.C. Hermanson, Ultrasonic measurement of condensate film thickness, J. Acoust. Soc. Am., 124(4), pp. EL196–EL202, 2008.
[20] S. Fiedler, S. Yildiz, H. Auracher, Determination of film thickness and flooding during reflux condensation in a small, inclined tube with an ultrasonic transducer, Int. J. Energy Res. 27 (4) (2003) 315–325.
[21] H. Zhao, D. Beysens, From droplet growth to film growth on a heterogeneous surface: condensation associated with a wettability gradient, Langmuir 11 (2) (Feb. 1995) 627–634.
[22] P. Dou, T. Wu, Z. Luo, Z. Peng, T. Sarkodie-Gyan, The application of the principle of wave superposition in ultrasonic measurement of lubricant film thickness, Meas. J. Int. Meas. Confed. 137 (2019) 312–322.
[23] O.F. Manfredi, R.S. Mills, M.M. Schirru, R.S. Dwyer-Joyce, Non-invasive measurement of lubricating oil viscosity using an ultrasonic continuously repeated chirp shear wave, Ultrasonics, 94, no. July 2018, pp. 332–339, 2019.
[24] L.E. Kinsler, A.R. Frey, A.B. Coppens, J.V. Sanders, Fundamentals of Acoustics, 4th ed., John Wiley & Sons Inc, 2000.
[25] D. Ensminger, L.J. Bond, Ultrasonics: Fundamentals, technologies, and applications, third edition, 2011.
[26] Y.A. Al-Aufi, B.N. Hewakandamby, G. Dimitrakis, M. Holmes, A. Hasan, N. J. Watson, Thin film thickness measurements in two phase annular flows using ultrasonic pulse echo techniques, Flow Meas. Instrum. 66 (2019) 67–78.